Integration of simulated moving bed chromatography and enzymatic racemization for the production of single enantiomers

Markus Fuereder, Christian Femmer, Giuseppe Storti, Sven Panke, Matthias Bechtold

Abstract

Integration of enantioseparation by simulated moving bed (SMB) and mild enzymatic racemization enables the production of single enantiomers from a racemic mixture in theoretically 100 % yield and hence overcomes the 50 % yield limitation of conventional SMB processes. We implemented such a process consisting of a Chirobiotic TAG column-SMB, an amino acid racemase-containing enzyme membrane reactor, and a nanofiltration unit for concentration of the distomer-enriched SMB raffinate prior to racemization on lab-scale for the production of enantiopure D-methionine. The integrated process scheme was operated continuously for over 30 hours without significant variations in product concentration and purity and with a yield of 93.5 %, demonstrating the feasibility of this integrated process concept. Furthermore, a rational analysis of the integrated process on the basis of a short-cut model was conducted. The process model consists of a true moving bed equilibrium stage model to represent the SMB, a continuous stirred tank reactor model with reversible Michaelis-Menten kinetics to represent the enzyme membrane reactor, a nanofiltration model and feed node mass balances, and enabled the identification of optimal operating points (flow rate ratios, enzyme concentration) at a variety of process specifications and objectives. Optimal operating points were calculated for different cost distributions between the applied materials such as stationary phase, enzyme, solvent, and nanofiltration membrane. By assigning plausible pricing data and lifetimes to the respective materials, variable costs for the specific process considered in this work were estimated.

1. Introduction

As the biological activity of chemical compounds can be drastically different depending on their stereoconfiguration, methods to obtain such molecules in enantiopure form are of high importance. The preferred method to obtain enantiopure preparations largely depends on the specific molecule to be synthesized. Efficient synthesis routes starting from cheap enantiopure precursors are often not readily available, and, despite the rapid progress in the field (Ager et al., 2012; Trost, 2004), the development of an asymmetric synthesis can be time consuming due to the challenging chemistry and the complexity of the development process (Blaser, 2002; Federsel, 2009). Consequently, a reaction sequence of less complicated non-enantioselective synthesis steps resulting in a racemic precursor and its subsequent enantiospecific resolution constitutes often the preferred synthetic strategy, despite the fact that the theoretical yield is limited to 50 % (Sheldon, 1996). Resolution can be achieved by a variety of methods including kinetic resolution and physical separation methods such as (diastereomeric or preferential) crystallization and chromatography. In particular, chiral chromatography – typically realized in continuous operating mode, such as through the simulated moving bed (SMB) technology – is widely used today for enantioseparations in the pharmaceutical sector due to the ability to design chromatographic processes rapidly and in conformity with regulations. Next, the use of SMB in chirotechnology is facilitated by an increasing selection of chiral stationary phases (CSP's) that enable the enantioseparation of the majority of racemates (Chankvetadze, 2012; Francotte, 2001).

In recent years a number of integrated process concepts have been proposed in order to increase productivity and to overcome the yield limitation of chromatography-based resolution processes. The optimization potential results from the fact that the throughput in chromatography can be increased when purity requirements are reduced (Blehaut and Nicoud, 1998). This was investigated in more detail by simulations, e.g. for the coupling of chromatography and crystallization with recycling of the residual mother liquor (Amanullah and Mazzotti, 2006; Gedicke et al., 2007), where the eutomer is first enriched to a suitable purity by a chromatographic step, and subsequently crystallized.

The yield limitation can be addressed similar to well established dynamic kinetic resolution processes (Ward, 1995) by racemization of the distomer. This can be realized inside of an SMB unit, e.g. by a pH gradient (Palacios et al., 2011), with side reactors as part of a multi-column chromatography process (Hashimoto et al., 1983), by integration of crystallization and racemization (Würges et al., 2009), or as a combination of chromatographic separations with an external reactor (Nimmig and Kaspereit, 2013).

In fact, a number of process combinations of chromatography, crystallization and racemization can be envisioned (Kaspereit et al., 2012). For selection of the optimal process structure a three step procedure has been proposed. First, a pre-selection of feasible processes based on qualitative criteria such as the availability of a racemization procedure and the type of phase diagram is conducted. In a next step the process variants are evaluated with short-cut models, followed by the process optimization of the most feasible concept (Kaspereit et al., 2012). Recently, the experimental implementation of a process for the production of 2,6-pipecoloxylidide by combining steady state recycling chromatography, crystallization, and racemization induced by an organometallic catalyst was reported (von Langermann et al., 2012). However, the process was operated such that the individual units were not directly coupled to each other for continuous operation.

Here we report the design and implementation of one of the promising process options in continuous operating mode: the integration of chiral SMB, recycle concentration by nanofiltration (NF), and enzymatic racemization for the production of enantiopure compounds in high yield (Fig. 1). As a model problem the production of D-methionine (D-Met) from racemic D,L-Met was chosen, since amino acids represent an important class of intermediates in the fine chemical industry (Leuchtenberger et al., 2005). Please note that such an installation can flexibly produce both enantiomers in high yield, depending only on which of the available ports is used for product removal. In principle, the NF unit can be placed at different positions in the process (Martin et al., 2015; Siitonen et al., 2015). The selected position has distinct advantages for EMR operation as it features the largest concentration difference and residence times.

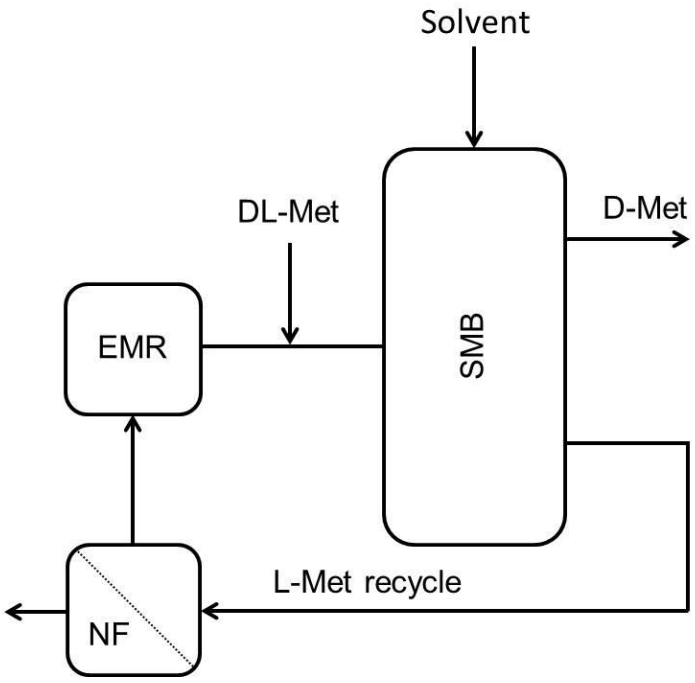

Fig. 1. Integration of chiral simulated moving bed (SMB) and mild enzymatic racemization for the production of D-Met. Racemic D,L-Met enters the process and is separated in the SMB. The stronger retained D-Met exits the process at the extract port of the SMB, while the undesired L-Met is concentrated using a continuous nanofiltration (NF) unit and enzymatically racemized in the enzyme membrane reactor (EMR) before it is combined with fresh feed.

Due to the direct coupling of units the same solvent needs to be applied in all unit operations. Hence, the design and optimization of a fully integrated production system requires a detailed characterization and parameterization of all involved units as a function of interoperable solvent (desorbent) compositions. In the case of the enzymatic racemization, function of the amino acid racemase (AAR) in water/methanol solvent systems was already demonstrated (Bechtold et al., 2007b). We also reported the suitability of teicoplanin aglycone, a macrocyclic glycopeptide as a CSP for the SMB separation of amino acids in a similar solvent environment (Bechtold et al., 2006; Fuereder et al., 2012). In the scope of this work the previously reported parameter values were applied in order to design and optimize the fully integrated process using a short cut process model. To our best knowledge this constitutes the first report on the experimental implementation of integration of chiral SMB and enzymatic racemization.

2. Theory

2.1. Integrated process model

For an *in silico* characterization of the integrated process, a model was developed, consisting of equations for each of the involved units and a node model connecting the units. Models were designed for the two most common production scenarios, differing in whether the earlier (here: L-Met) or the later (here: D-Met) eluting enantiomer is considered as the product. For the sake of simplicity and speed of optimization, steady state operation was assumed in all models. A schematic representation of the integrated process is depicted in Fig. 2.

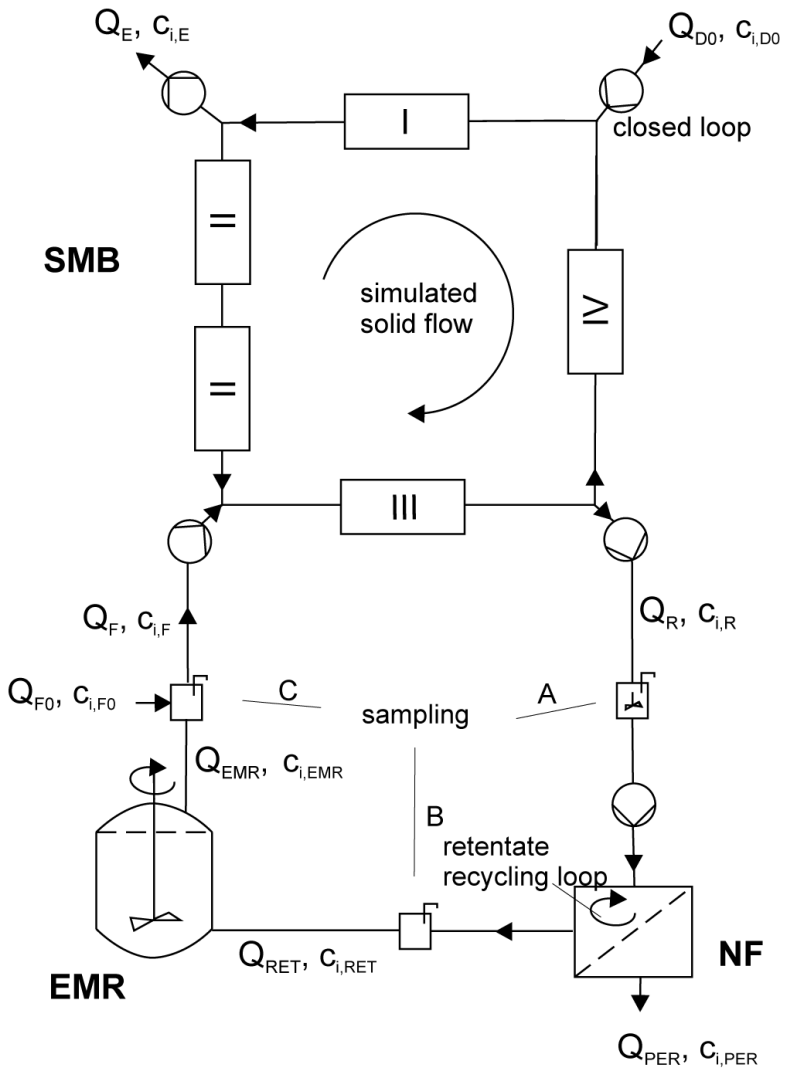

Fig. 2. Schematic representation of the experimental setup of the integrated process for the production of D-methionine from racemic methionine. The nanofiltration (NF) was operated with a recycling loop on the retentate side, as schematically indicated in the figure.

2.1.1. SMB

SMB operation is described by a true moving bed (TMB) model using an equilibrium stage model (Biressi et al., 2000; Kaspereit et al., 2012; Martin and Synge, 1941) for representation of the chromatographic process. The TMB unit is divided in 4xN discrete volumes (so-called equilibrium stages) of ideal mixing and equilibration while each one of the four zones *j* is represented by N stages. The generic stage *k*, where no combination with outer flow rates occurs, is described by the following material balance:

$$0 = q_{i,k+1} - q_{i,k} + m_j \left(c_{i,k-1} - c_{i,k} \right) \qquad i = (1,2),\ j = (1,..,4),\ k = (1,\ldots,4N)\,, \tag{1}$$

where m_j is a dimensionless flow rate ratio (liquid over solid flow) and the concentration in the stationary phase q_i of each component *i* (*i* = 1 for the less retained component, L-met, and *i* = 2 for the most retained component, D-Met) is assumed to be in equilibrium with the mobile phase concentration c_i. There are four distinct stages, which are the first stages in each zone, where the inlet and outlet streams (desorbent *D0*, extract *E*, feed *F*, and raffinate *R*) are injected or withdrawn, respectively. Note that these equilibrium stages are merged with the material balances for the nodes between the zones.

First stage in zone 1 (desorbent stage):

$$0 = q_{i,2} - q_{i,1} + m_4 c_{i,4N} - m_1 c_{i,1} + (m_1 - m_4) c_{i,D0}\,. \tag{2}$$

First stage in zone 2 (extract stage):

$$0 = q_{i,N+2} - q_{i,N+1} + m_1 c_{i,N} - m_2 c_{i,N+1} - (m_1 - m_2) c_{i,E}\,. \tag{3}$$

First stage in zone 3 (feed stage):

$$0 = q_{i,2N+2} - q_{i,2N+1} + m_2 c_{i,2N} - m_3 c_{i,2N+1} + (m_3 - m_2) c_{i,F}\,. \tag{4}$$

First stage in zone 4 (raffinate stage):

$$0 = q_{i,3N+2} - q_{i,3N+1} + m_3 c_{i,3N} - m_4 c_{i,3N+1} - \left(m_3 - m_4\right) c_{i,R}\,. \tag{5}$$

The mobile phase concentration c_i is given by a bi-Langmuir isotherm with six parameters (Fuereder et al., 2012):

$$q_i = q_{sI} \frac{b_{Ii} c_i}{1 + b_{I1} c_1 + b_{I2} c_2} + q_{sII} \frac{b_{IIi} c_i}{1 + b_{II1} c_1 + b_{II2} c_2} \tag{6}$$

The translation of TMB flow rate ratios to external SMB flow rates Q is described by Eqs. (7)-(10). By setting the switch time t^*, column volume V_C and porosity ε, the external SMB flow rates can be calculated by (Mazzotti et al, 2006):

$$Q_{D0} = \frac{1}{t^*}(1-\varepsilon)V_C(m_1 - m_4), \quad \textbf{(7)}$$

$$Q_E = \frac{1}{t^*}(1-\varepsilon)V_C(m_1 - m_2), \quad \textbf{(8)}$$

$$Q_F = \frac{1}{t^*}(1-\varepsilon)V_C(m_3 - m_2), \quad \textbf{(9)}$$

$$Q_R = \frac{1}{t^*}(1-\varepsilon)V_C(m_3 - m_4). \quad \textbf{(10)}$$

2.1.2. NF

The NF unit is modeled employing material balances with Q_{RET} and Q_{PER} as retentate and permeate flow rates and a single parameter, the rejection REJ, as a function of the solute concentrations $c_{i,RET}$ and $c_{i,PER}$ in the retentate and permeate streams. Eqs. (11 b) and (12 b) reflect the case with L-Met as the product. In the case of chiral solutes the rejection is equal for both enantiomers.

$$Q_R = Q_{RET} + Q_{PER} \quad \textbf{(11 a)}$$

$$Q_E = Q_{RET} + Q_{PER} \quad \textbf{(11 b)}$$

$$Q_R c_{i,R} = Q_{RET} c_{i,RET} + Q_{PER} c_{i,PER} \quad \textbf{(12 a)}$$

$$Q_E c_{i,E} = Q_{RET} c_{i,RET} + Q_{PER} c_{i,PER} \quad \textbf{(12 b)}$$

$$REJ_i = 1 - \frac{c_{i,PER}}{c_{i,RET}} \quad \textbf{(13)}$$

2.1.3. EMR

The racemization in the EMR is described by a continuous stirred tank reactor (CSTR) model for steady state operation, with the underlying assumption of constant volumetric inlet and outlet flow rates (Eq. (14)-(16)). The enzyme kinetics are described by reversible Michaelis-Menten kinetics (15) with the equilibrium constant being K_{eq}=1 as the reaction cannot proceed beyond the racemic

composition. Hence, the reaction kinetics can be fully described by the catalytic constant k_{cat} and two affinity constants $K_{M,i}$ for forward and backward reaction.

$$Q_{RET}c_{1,EMR} = Q_{RET}c_{1,RET} - rV_{EMR} \quad \textbf{(14)}$$

$$r = \frac{k_{cat}}{K_{M,1}}c_{ENZ}\frac{c_{1,EMR} - \frac{c_{2,EMR}}{K_{eq}}}{1 + \frac{c_{1,EMR}}{K_{M,1}} + \frac{c_{2,EMR}}{K_{M,2}}} = \frac{k_{cat}}{K_{M,1}}c_{ENZ}\frac{c_{1,EMR} - c_{2,EMR}}{1 + \frac{c_{1,EMR}}{K_{M,1}} + \frac{c_{2,EMR}}{K_{M,2}}} \quad \textbf{(15)}$$

$$c_{2,EMR} = c_{1,RET} + c_{2,RET} - c_{1,EMR} \quad \textbf{(16)}$$

2.1.4. Feed node

The feed node, where fresh feed is combined with the reactor effluent, is described with mass balances for the fluid and the solutes. The dilution factor δ is introduced as the ratio of recycled total concentration (i.e. the sum of the concentrations of both enantiomers) and the total fresh feed concentration (19).

$$Q_F = Q_{F0} + Q_{RET} \quad \textbf{(17)}$$

$$Q_F c_{i,F} = Q_{F0}c_{i,F0} + Q_{EMR}c_{i,EMR} \quad \textbf{(18)}$$

$$c_{1,EMR} + c_{2,EMR} = \delta(c_{1,F0} + c_{2,F0}) \quad \textbf{(19)}$$

2.2. Performance indicators, objective and cost functions

The performances of the integrated process have been quantified by the different parameters defined below. The throughput *TP* of the integrated process is defined as the amount of product that is yielded per unit time. Depending on which enantiomer is targeted as product, *TP* is calculated by the L-Met mass flow in the raffinate (20) or the D-Met mass flow in the extract (21).

$$TP_1 = Q_R c_{1,R} \quad \textbf{(20)}$$

$$TP_2 = Q_E c_{2,E} \quad \textbf{(21)}$$

The desorbent requirement *DR* is calculated as the amount of desorbent required per amount of D- or L-Met produced,

$$DR_i = \frac{Q_{D0}}{TP_i} \quad . \tag{22}$$

The productivity *PR* is defined as *TP* divided by the mass of CSP,

$$PR_i = \frac{TPi}{M_{CSP}} \quad , \tag{23}$$

the enzyme requirement *ER* is defined as the amount of enzyme required per amount of D- or L-Met produced in time

$$ER_i = \frac{c_{ENZ} V_{EMR}}{TP_i} \quad , \tag{24}$$

and the membrane requirement *MR* is defined as the membrane area A_{NF} required per *TP*

$$MR_i = \frac{A_{NF}}{TP_i} \quad . \tag{25}$$

The overall yield for the integrated process is defined as the ratio of *TP* and the mass flow of racemic methionine fed to the system,

$$Y_i = \frac{TP_i}{Q_{F0}(c_{1F0} + c_{2F0})} . \tag{26}$$

The purity (*PU*, in %) at the extract and raffinate port is given by:

$$PU_E = 100 \frac{c_{2,E}}{c_{1,E} + c_{2,E}} \tag{27}$$

$$PU_R = 100 \frac{c_{1,R}}{c_{1,R} + c_{2R}} \quad . \tag{28}$$

The conversion in the EMR (*X*) is defined as the ratio of target enantiomer concentration leaving the EMR and the overall methionine concentration entering the unit

$$. \; X_i = \frac{c_{i,EMR}}{c_{1,RET} + c_{2,RET}} \tag{29}$$

In order to illustrate the trade-off between the conflicting objectives OF_x (*1/TP, DR, 1/PR, ER*) , two- and three-dimensional multi-objective Pareto optimizations were performed (Bhaskar et al., 2000; Paredes and Mazzotti, 2007). Optimal operating points were obtained by minimizing function *f* with the structure

$$f = \sum_x w_x OF_x \ . \qquad \textbf{(30)}$$

The weight factors w_x were varied in different increments between 0 and 1 such that

$$\sum_x w_x = 1 \ . \qquad \textbf{(31)}$$

3. Experimental

3.1. Chemicals

Methionine, methanol, ammonium acetate (NH_4Ac) and acetonitrile were supplied by Sigma–Aldrich Chemie GmbH (Buchs, Switzerland). All organic solvents were HPLC grade and water was deionized. Solvent composition is given in % (v/v) unless specified otherwise.

3.2. Enzyme preparation

The procedure for cultivating *Escherichia coli* JM109 cells overproducing AAR (EC 5.1.1.10) from *Pseudomonas putida* DSM 3263 has been described before (Bechtold et al., 2007b). To obtain an enzyme preparation, cells were harvested by centrifugation and resuspended in aqueous buffer (50 mM NH_4Ac, 40 µM pyridoxal-5-phosphate (PLP), adjusted to pH7 with ammonium hydroxide solution) to a concentration of 100 g cell wet weight (CWW) L^{-1}. This suspension was disrupted in a high-pressure homogenizer (Haskel Hochdrucksysteme GmbH, Wesel, Germany) at a 1'200 bar pressure drop over the orifice. The supernatant of the ensuing centrifugation (30 min, 3 x 10^4 g, 4°C) was incubated overnight on ice to guarantee complete saturation of the enzyme's active site with its cofactor PLP provided by the aqueous buffer, and then represented cell free extract (CFX) and was distributed in aliquots for storage at -80°C. One unit (U) of AAR was defined as the amount of enzyme producing 1 µmol min^{-1} of D-Met starting from 100 mM L-Met at 25 °C and pH 7.0. The CFX contained 1,965 U mL^{-1} and 24 mg mL^{-1} of total protein. Of this, approximately 4.2 mg mL^{-1} was AAR, as determined by densitometric analysis of a Coomassie stained SDS-polyacrylamide gel (Sambrook and Russell, 2001).

3.3. Analytics

Concentrations of L- and D-Met were determined using a stainless steel Chirobiotic TAG column (250 mm x 4.6 mm ID) (Sigma-Aldrich Corp., USA) on an Agilent 1100 HPLC system equipped with a diode array detector at a wavelength of 220 nm. A mobile phase containing 75/25 5 mM NH_4Ac pH 6/methanol at a flow rate of 1 mL min^{-1} was used. The injected sample volume was 10 µL.

3.4. SMB operation

SMB experiments were performed on a modified ÄKTA system (GE Healthcare, Freiburg, Germany) using 5 stainless steel Chirobiotic TAG columns (100 mm x 10 mm ID) (Sigma-Aldrich Corp., US) in 1-2-1-1 closed loop configuration. The laboratory SMB-setup has been explained in detail previously (Fuereder et al., 2012). The extra-column dead volume V_{Dj} of each zone was 0.1 mL.

3.5. NF

In order to concentrate the raffinate leaving the SMB, a customized cross-flow NF unit (MMS AG, Switzerland) was employed. An integrated gear pump (Scherzinger, Furtwangen, Germany) ensured a cross flow rate of 1.2 L min^{-1} in order to mitigate concentration polarization and fouling. A polyamide membrane with a molecular cut-off of around 90 Da (NF-90, Dow FILMTEC^{TM}, US (Zhu et al., 2007)) and a maximum operating pressure of 60 bar was used.

The NF feed flow was provided using a Merck L-6200A HPLC pump (VWR, Nyon, Switzerland). The maximum pressure limit of the pump was set to 40 bar to accommodate the pressure limitation of the NF. NF operation was maintained at 25˚C. Depending on the concentration of the raffinate, the required volume concentration factor *VCF* (ratio of raffinate over retentate flow rate) to achieve the required retentate concentration was determined. The retentate flow rate was set and controlled online using a LIQUI-FLOW flow controller (Bronkhorst, Reinach, Switzerland). The NF unit was pre-filled with 13.6 g L^{-1} L-Met in 75/25 (v/v) 5 mM NH_4Ac pH 6/methanol to reduce the start-up time before integration. Prior to closing the recycle stream the retentate and permeate outlets were collected and weighed to determine the exact flow rates. The outlet samples were analyzed by HPLC to determine *REJ* and *VCF*.

3.6. EMR operation

Racemization of the concentrated recycled methionine leaving the NF unit was carried out in an EMR (Bioengineering AG, Switzerland) with an inner volume of 10 mL with a magnetic stirrer set at 600 rpm. A polyethersulfone membrane filter (Sartorius Stedim, Tagelswangen, Switzerland) with a cut-off of 10 kDa was used to retain the AAR. Prior to connection with the NF and SMB unit, the EMR

was equilibrated by feeding with 13.6 g L^{-1} L-Met in 75/25 5 mM NH_4Ac pH 6/methanol at a flow rate of 0.3 mL min^{-1}. The CFX was injected using a rheodyne manual sample injector (Ercatech, Bern, Switzerland). Before the connection of the EMR to the NF and SMB, EMR outlet samples were analyzed to check for conversion and potential enzyme leakage.

3.7. Integrated process setup and start-up

The applied integrated process is depicted in Fig. 2. Three sampling stations were installed between the different units: between SMB and NF, a stirred vessel (A) was used as sampling device for sampling and verifying that the NF feed pump had the same or slightly higher flow rate (to balance the sample volume taken) at its suction side as the SMB raffinate pump delivered. Between NF and EMR and between EMR and SMB, different micro-splitter valves (Ercatech AG, Switzerland) were used for sampling (B and C, respectively, Fig. 2).

The start-up of the integrated process was conducted in three steps. First, the SMB was started and operated until steady state was reached which was confirmed by closing the mass balance on the basis of HPLC quantification of raffinate and extract concentrations. Meanwhile, the NF and the EMR were pre-equilibrated with the expected process conditions as described above. Next, the SMB and the NF were coupled through sampling device A. The NF feed pump was set to the flow rate of the raffinate which had been measured during SMB operation in the previous step. Finally, the reactor inlet was coupled with the NF retentate and the reactor outlet was connected with the feed node. Thus, SMB, NF and EMR were connected in closed loop arrangement for the fully integrated operation. Samples of the product stream (extract), raffinate, permeate and EMR effluent were analyzed at regular time intervals. The SMB and the EMR were kept inside a temperature chamber to maintain a constant temperature of 22˚C, while the temperature in the NF was controlled by an external water bath set to 25°C. An online degasser ensured the degassing of fresh and recycled eluent and feed entering the SMB system.

3.8. *In silico* procedures

The integrated process model was implemented in the GAMS modeling environment (GAMS, Washington DC, USA) and simulations were carried out with the parameter set given in Table 1 unless stated otherwise. The minimum product purity (PU_E or PU_R) was fixed at 99.5% unless stated otherwise.

Table 1: Parameters and fixed variables for the integrated process simulations.

Parameters						Fixed variables	
V_C	7.85 mL	q_{sI}	68 g L^{-1}	$K_{M,1}$	1.41 g L^{-1}	$c_{F0,i}$	7.5 g L^{-1}
E	0.651	q_{sII}	1.28 g L^{-1}	$K_{M,2}$	2.37 g L^{-1}	$c_{D0,i}$	10^{-9} g L^{-1}
V_D	0.1 mL	b_{I1}	0.02 L g^{-1}	k_{cat1}	6.9 min^{-1}	c_{ENZ}	4.2 g L^{-1}
t^*	2 min	b_{I2}	0.03 L g^{-1}	REJ	0.985	V_{EMR}	10 mL
N	48	b_{II1}	0.28 L g^{-1}			δ	1
		b_{II2}	1.87 L g^{-1}				

The parameters for the bi-Langmuir isotherm model have been determined previously using the perturbation method at 25% methanol concentration and 22°C (Fuereder et al., 2014), as have been the parameters for the reversible Michaelis-Menten kinetics (Bechtold et al., 2007b). Enzyme concentration and the dilution factor δ were fixed at the value given in Table 1 unless stated otherwise. In all cases the mass balance for the overall process and all involved units closed with a deviation less than 0.03 % with respect to the respective feed mass flow.

4. Results and Discussion

The integration of chiral SMB, NF and EMR for the production of single enantiomers from a racemate constitutes a novel process. A proof of concept run using a lab-scale setup and straightforward design rules was conducted to demonstrate the principle feasibility of the process. The complexity of the integrated setup makes it difficult to understand all intricacies of the process intuitively. Therefore model-based analysis using a short-cut model of the integrated process was applied to identify the potential for process improvement for different (cost) scenarios.

4.1. Experimental proof of concept

The experimental implementation of the integrated process was realized for the production of D-Met on a lab-scale plant using an ÄKTA-based SMB (max. 10 mL min^{-1} flow rate), a crossflow NF unit with a membrane area of 28 cm^2 and a 10 mL EMR. Briefly, the SMB raffinate stream containing primarily the distomeric L-Met was directed to the NF unit. The concentrated NF retentate stream served as feed for the EMR where the racemase enzyme catalyzed the interconversion of L- and D-enantiomers. The reactor effluent was combined with fresh racemic feed and fed to the SMB unit. The product D-Met was obtained from the SMB extract port.

Similar to recent work (Wagner et al., 2012) we used a simplistic design approach for the proof of concept run. Using the well-established short cut design for SMB separation with Bi-Langmuir isotherms (Gentilini et al., 1998) suitable operating points for SMB operation were identified. With the SMB operating points and, as a result, the external SMB flow rates set, the NF flow rates were calculated depending on the desired concentration factor. In this case, the retentate flow rate was adjusted such that the dilution factor δ was 0.9, resulting in a total retentate concentration of 13.6 g L^{-1}, which is lower than the fresh feed concentration c_{F0} of 15 g L^{-1}. This was done as a precaution in order to ensure that methionine could not precipitate in the NF as its solubility in the applied solvent mixture is only slightly above the set fresh feed concentration of 15 g L^{-1} (Fuereder et al., 2014); the influence of the feed node dilution factor on overall process performance is discussed in 4.2.2.2. With the flow rate and the reactor volume fixed the degree of conversion in the EMR can only be influenced by the amount of enzyme supplied to the reactor. For the proof of principle a constant conversion close to racemic concentration was targeted which was achieved by loading the EMR with an excess of AAR (> 6,000 U). The large excess of enzyme was applied in order to realize an experimentally simple solution to compensate for enzyme degradation that was previously reported for this enzyme under elevated methanol concentrations (Bechtold et al., 2007b) and thus to ensure constant conversion over time. The proof of concept-run was performed for 33 hours yielding virtually invariant process performance over the entire time period. Note that dynamic effects were not studied as all units were pre-equilibrated close to the expected steady-state conditions before coupling. Towards the end of the experiment, a slight decrease of raffinate purity and an increase in extract purity was observed. This behavior can theoretically originate from deviations in the set process conditions such as a diminished retentate flow rate which would result in an increase in feed concentration and consequently in a shift of the area of complete separation in the m_2-m_3 plane towards lower m_2-m_3 values. A similar shift can be assumed when overall retention is decreased, a phenomenon often associated with column aging. However, the deviations are rather small, and hence the proposed explanations should be considered as speculative. Overall, the constant concentrations obtained at the SMB, NF and EMR outlet ports (Fig. 3) clearly indicate stable operation which is particularly remarkable considering a chromatographic process that is characterized by highly non-linear isotherms (Fuereder et al., 2014) and a memory effect (Bechtold et al., 2007a; Fuereder et al., 2012)

Next, a yield of 93.5 % was obtained clearly demonstrating that process integration allows the conversion of the racemate to the single enantiomer to be increased far beyond the 50% yield limitation of a stand-alone SMB. The difference to a yield of 100 % can be attributed to the incomplete rejection of 0.985 of the NF membrane (4.5% of the fed amino acid left the process in the NF permeate) and the limited purity of 98% of the extract (2% L-Met in the extract). The product loss

in the retentate can be minimized by operating the SMB with low dilution of the extract (at the expense of productivity) and hence lowering the required permeate stream. Alternatively, different membrane materials (e.g. reverse osmosis membrane, at the expense of a higher pressure drop in the filtration step) can be employed that will provide in theory a complete rejection of methionine. Finally, a *TP* of 3.6 g of D-Met per day was obtained and *DR* was 0.97 L per g of D-Met in the product stream.

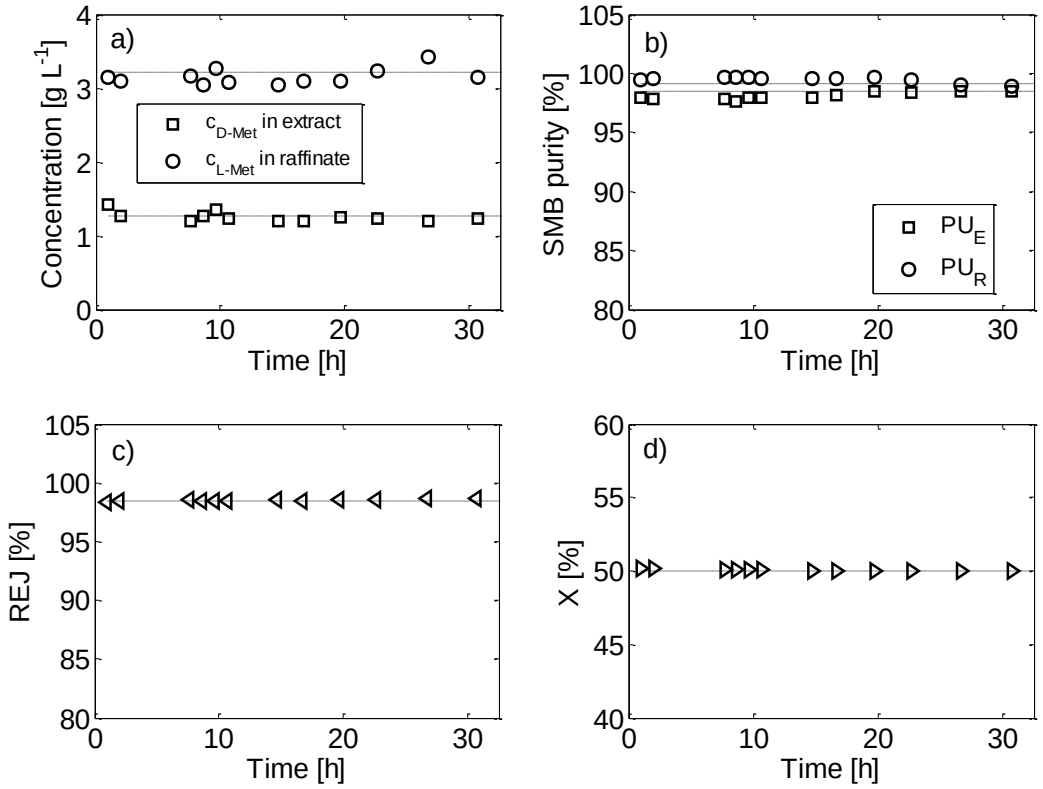

Fig. 3. Integrated process operation for 30 hours: a) Concentrations of the enriched enantiomers at the respective SMB outlets. b) SMB outlet purities. c) NF rejection. d) EMR conversion. Symbols refer to experimental values, dashed lines to expected values from process design.

4.2. Model based analysis of the integrated process

Having demonstrated the technical feasibility of the integrated SMB-NF-EMR process, we addressed the development of an efficient design procedure using the previously presented steady state integrated process model. The required parameterization for the chromatographic process (adsorption isotherms) and the reactor (enzyme kinetics) had been determined previously and their

ability to correctly describe stand-alone operation demonstrated (Fuereder et al., 2012; Bechtold et al., 2007b). For determining NF rejection, long-term test runs at various *VCF* and retentate concentrations were conducted and showed stable rejection of 0.985 (data not shown). In the following chapters this value was assumed to be constant with varying flow rates for the sake of simplicity.

Similar to SMB operation, also in an integrated process the distribution of variable costs determines the optimal operation; therefore detailed pricing data is required for optimal process design. SMB performance is typically described by two process metrics: (i) specific productivity, which reflects product or feed mass flow referenced to the volume or mass of stationary phase and (ii) desorbent requirement, usually defined as the volumetric feed streams to the SMB referenced to the *TP* of the system. Typically, these two criteria are conflicting (Rajendran et al., 2009). In order to cover the complete range of possible scenarios, multi-objective optimizations based on Pareto sets (Bhaskar et al., 2000) can be employed (Paredes and Mazzotti, 2007; Amanullah and Mazzotti, 2006). In this work we use multi-objective optimization in order to analyze the integrated process. Since the SMB unit is embedded and connected with two more units, the approach presented here features cost-related metrics that originate from the variable costs of each unit.

When comparing the integrated process to a conventional SMB process, the major difference from a design perspective is that the purity of the distomer-enriched outlet changes from a value that has to be specified for yield reasons to a free variable. Therefore, we start by investigating the impact of reduced recycling purities on the integrated process.

4.2.1. Relaxed purity constraints at the distomer outlet

It was demonstrated previously (Kaspereit et al., 2002; Kaspereit et al., 2007) that stand-alone SMB operation with a lowered outlet purity constraint can be significantly improved and more feed can be processed. In the integrated process installation the high purity requirement on the distomer outlet does not apply anymore due to recycling, and in the theoretical case of total rejection of the solute in the NF a yield of 100% can be reached even if the purity of the distomer at the respective outlet is lowered. In order to elucidate the effect of the recycle purity on yield, *TP,* and *DR*, a parametric analysis was performed for either enantiomer as product. More specifically, for the objectives *TP* and *DR* optimal operating points were calculated at different recycling purities, and the influence on the yield was analyzed.

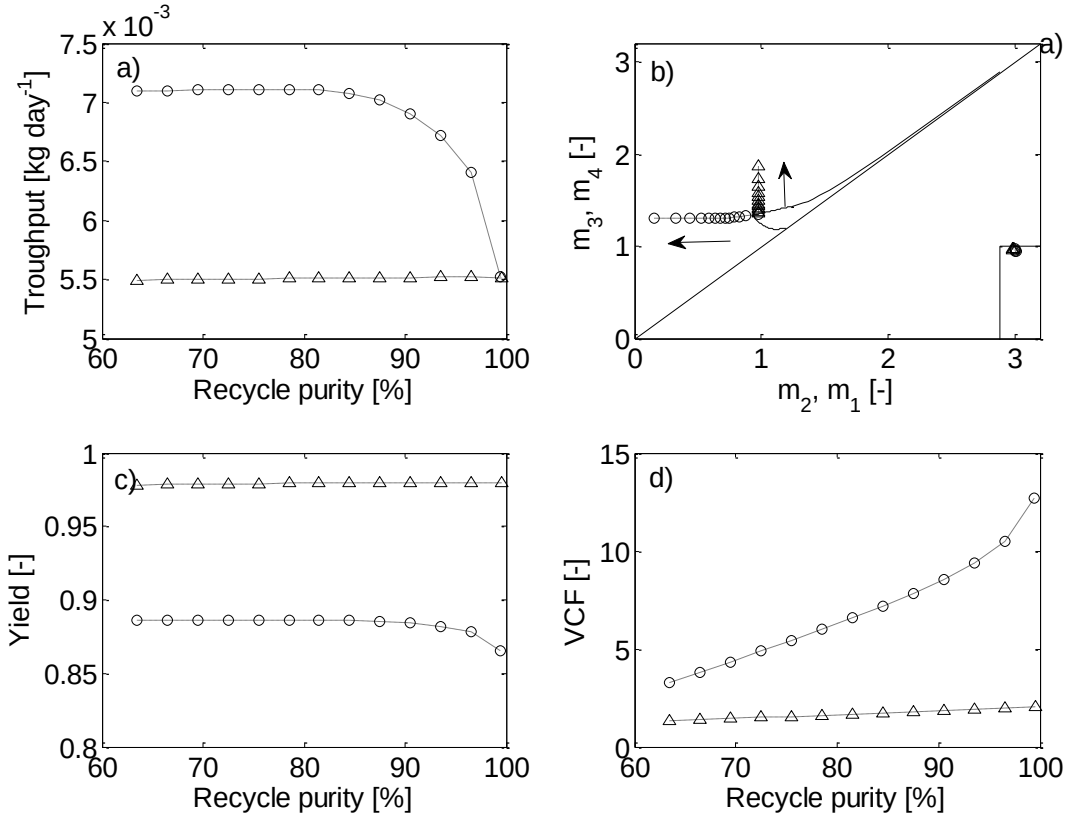

Fig. 4. Throughput *TP* of the integrated process for the production of D-Met (triangle) and L-Met (circles) at different recycle purities. The objective was to minimize *1/ TP*. a) Development of *TP* at different recycling purities. b) Development of optimal m-values in the m_2-m_3 plane and the m_1-m_4 plane. The arrows indicate the direction of lowered recycling purity. The lines represent complete separation regions derived from triangle theory for Bi-Langmuir isotherms (Gentilini et al., 1998). c), d) Development of associated yield values and volume concentration factors (*VCF*, ratio of raffinate over retentate flow rate) at different recycle purities.

While for the production of D-Met no significant increase in *TP* is obtained (Fig. 4a) with lower recycle purities, *TP* for L-Met can be significantly improved. This behavior can be explained by the internal SMB concentration profiles which show a shock layer (sharp front) in the direction of fluid flow and a dispersive wave at the rear. In case the target enantiomer is the less retained component (here L-Met), m_2 can be lowered significantly without increasing the eutomer concentration too much due to the dispersive character of the concentration profile at the extract port. Consequently, extract purity will be only slightly compromised by an increase in m_2. The increase in mass flow into the system (as m_3-m_2 increases correspondingly) is favorably split up with the eutomer directed to the raffinate port and the distomer to the extract port, hence throughput increases without

compromising the purity at the product port (here L-Met at the raffinate port). The situation is opposite when considering the more retained compound as product: due to the sharp front at the raffinate port increasing m_3 will direct the excess eutomer mostly to the raffinate outlet, so that hardly any net gain in throughput is achieved at the extract outlet. The overall yield of both process options is a function of the concentrations and compositions at the distomer outlet. Low concentrations require a higher *VCF*. With a constant rejection in the NF of 0.985 more material gets lost through the permeate stream at higher *VCF*. Since the concentrations at the extract port are usually lower than at the raffinate port, the overall yield for the production of D-Met is higher than for the production of L-Met (Fig. 4c and d).

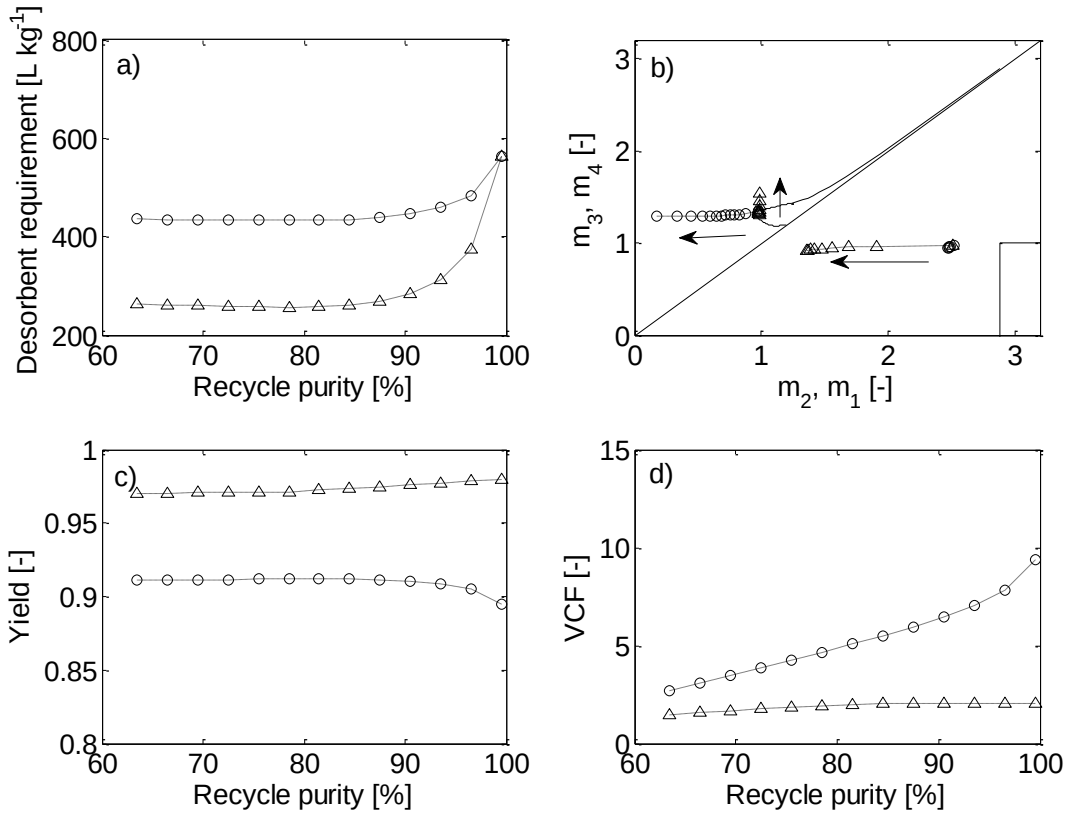

Fig. 5. Desorbent requirement *DR* of the integrated process for the production of D-Met (triangles) and L-Met (circles) at different recycle purities. The objective was to minimize *DR*. a) Development of *DR* at different recycling purities. b) Development of optimal m-values in the m_2-m_3 plane and the m_1-m_4 plane. The arrows indicate the direction of lowered recycling purity. The lines represent complete separation regions derived from triangle theory for Bi-Langmuir isotherms (Gentilini et al., 1998). c) and d) development of associated yield values and d) volume concentration factors (*VCF*, ratio of raffinate over retentate flow rate) at different recycle purities.

When optimizing for *DR* (Fig. 5), the variable that has the largest influence on the production of D-Met is m_1. With lowered m_1 the dispersive rear end of D-Met concentration profile is carried over to Zone 4 and ends up in the raffinate, but with only moderate effect on the raffinate purity, leading to a significant reduction of *DR*. In the case of L-Met production, the situation is similar to the case when optimizing for *TP*. Again, m_2 is affected as the main variable; however m_1 is at a slightly lower level when optimizing for *DR* compared to *TP*.

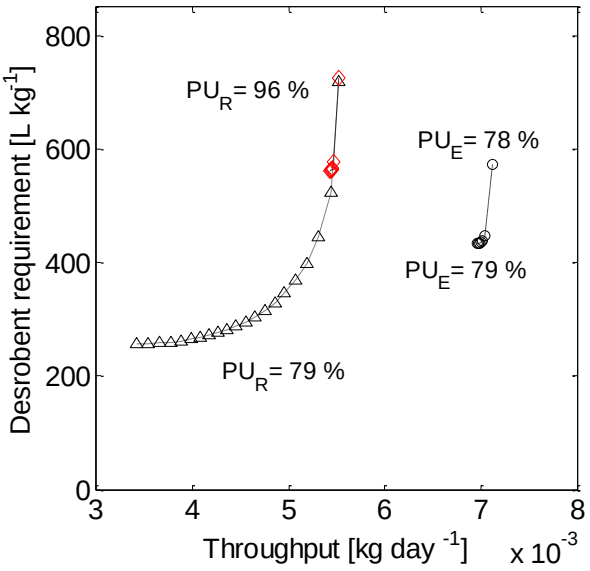

Fig. 6. Pareto sets for integrated process for the production of D-Met (triangles) and L-Met (circles). The recycling purities PU_E (extract purity) and PU_R (raffinate purity) for the extreme cases are given as numbers. Red diamonds: Pareto set with a minimal purity of the recycle stream of 99.5 %.

This behavior is also reflected in a Pareto set with *DR* and *TP* as conflicting functions (Fig. 6). While for the case of D-Met production the objectives are conflicting and different optimal raffinate purities result, there is almost no conflict in the case of L-Met production.

The potential benefit of reduced recycling purities can be best illustrated by comparison with similar calculations for high purity scenario (recycling purity and product purity specified to 99.5%). Due to the symmetric purity restriction, the Pareto curve is the same regardless of whether the product is obtained at the raffinate or at the extract port. The calculated Pareto curve indicates a very moderate tradeoff between maximum *PR* and DR (Fig. 6 red diamonds) and is situated very closely to the high *TP* part of the Pareto curve calculated for D-Met as product. In consequence, the reduced recycling purity option will not improve performance significantly when *TP* is the dominating optimization parameter while a moderate to drastic *DR* improvement can be obtained - depending

on the actual impact of *DR* compared to *TP*. Considering the case of "product in raffinate", allowing for reduced recycling purity shifts the Pareto set to higher *PR* and lower *DR* and hence improves operation for all optimization scenarios.

It is worth noting that the investigated process scenario with very high enzyme concentration and hence full conversion to the racemic mixture in the EMR is formally equal to the investigation of a stand-alone SMB system. However, the applied objective functions differ from traditional SMB investigations (Rajendran et al., 2009), where typically both enantiomers are considered as product and hence SMB analysis on the basis of how much target enantiomer can actually be obtained from the product port is still lacking.

For the remainder of this work, the distomer purity constraint is relaxed, and the system further inspected with respect to process specifications for D-Met production.

4.2.2. Process specifications

4.2.2.1. Product purity

After analyzing the effects of relaxed purities at the distomer outlet, the effect of the product purity requirement on *TP*, *DR* and yield was analyzed. To this end we performed Pareto optimization with *TP* and *DR* as conflicting objectives at different required product purities. The results clearly demonstrate that *TP* as well as *DR* improve with decreasing purity requirement (Fig. 7). On the other hand the yield decreases since obviously higher amounts of distomer are lost over the product port at decreased product purity. In Fig. 7, the experimental operating point with a product purity of 98% is compared to the in-silico results, demonstrating the general potential for improvement of TP and DR when using optimal recycling purities and m-values. It should be noted however, that theoretical and experimental operating points can only be roughly compared here, since the feed node dilution factor δ in the experimental run was set to 0.9 (as mentioned above). The effect of a dilution factor of less than 1 is discussed in the next section.

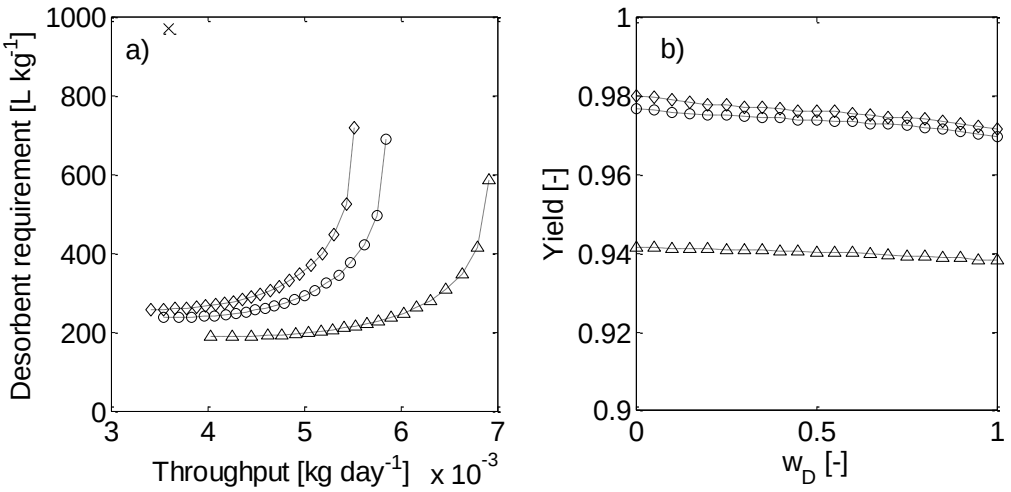

Fig. 7. Effect of the product purity on process performance parameters *TP, DR,* and *Y*. a) Pareto optimization at different product purities. b) Effect of product purity on yield at different desorbent weight factors w_D (Eq. 33). Diamonds: PU_E= 99.5%, circles: PU_E=99%, triangles: PU_E=95%. Cross: experimental proof of concept run with a product purity of 98%. Please note that the feed node dilution factor δ was set to 0.9 in the experimental run and the model results were calculated using a δ of 1.

4.2.2.2. Feed node dilution

Next, we addressed the second important process specification, namely the relationship between the overall feed concentration and the reactor effluent concentration that is expressed as the dilution factor δ. For $\delta = 1$ the total concentration leaving the reactor is equal to the feed concentration. This is a limiting case as the feed concentration is assumed to be close to the solubility limit. On the other hand the process can be more easily operated with a dilute reactor effluent with respect to the feed stream, e.g. the experimental proof of concept was operated with a δ of 0.9. A parameter study with relaxed purity constraints and varying δ shows that a lower δ decreases *TP* and increases *DR* (Fig. 8), but has a moderately beneficial effect on the yield because of the decreased required *VCF*.

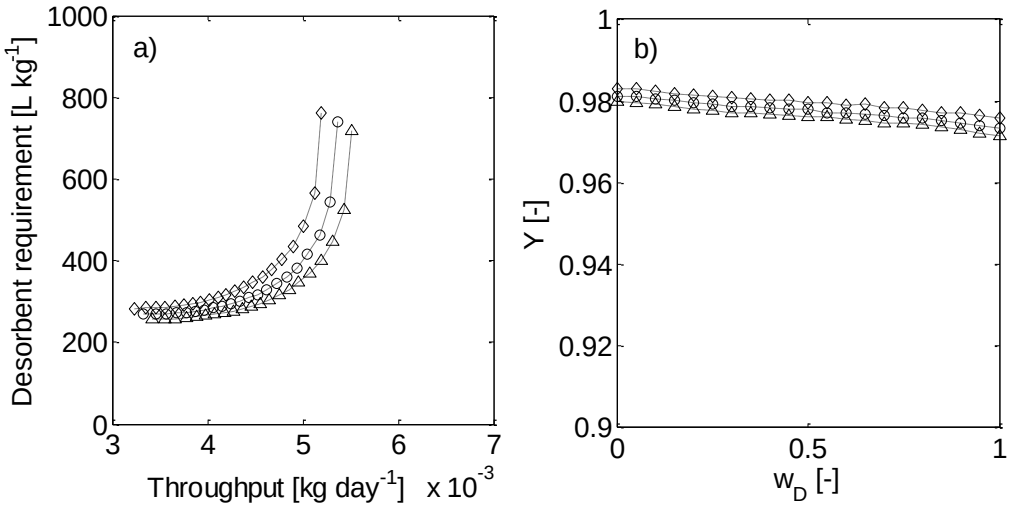

Fig. 8. Effect of the feed node dilution factor δ on the process performance parameters *TP*, *DR*, and *Y*. a) Pareto optimization at varying δ. b) Effect of δ on yield at different desorbent weight factors w_D. (Eq. 33). Triangles: δ=1, circles: δ=0.9, diamonds: δ=0.8.

4.3. Cost analysis

In this section we focus on variable costs only, thus neglecting investment costs. This is considered a reasonable approximation to identify and understand the main cost items, even though the estimated costs do not constitute a complete economical evaluation of the process.

4.3.1. Cost functions

The objective function should reflect all variable costs associated with the production. Accordingly, a cumulative cost function accounting for contributions from enzyme, stationary phase, membrane and solvent consumption and specific to the product throughput is considered:

$$PC = \frac{M_{ENZ}\pi_{ENZ}}{TP_i} + \frac{M_{CSP}\pi_{CSP}}{TP_i} + \frac{M_{NFM}\pi_{NFM}}{TP_i} + \frac{M_D\pi_D}{TP_i} \quad \textbf{(32)}$$

The exact contribution of the respective consumable to the global cost function depends on the specific cost per unit time π_x and the amount required in the process M_x. We define here $\pi_{x,}$ as the ratio of price P_x and life-span l_x, which can vary significantly for each of the unit operations (Table 2). If accurate data on the specific costs are available for all applied materials, a single solution can be obtained by optimizing for overall variable costs. However, the estimation of life-spans e.g. in the

case of the CSP is difficult and involving large uncertainty. Further, optimal solutions obtained for a wide range of possible cost scenarios provide much more information and can identify ranges of elevated sensitivity.

By dividing (Eq. 32) by the sum of the specific costs, the cost function *f* can be expressed as a combination of cost-related process metrics (*PR, ER, MR, DR*) and dimensionless weight factors *w:*

$$f = w_{ENZ} ER + w_{CSP} \frac{1}{PR} + w_{NFM} MR + w_D DR', \quad \textbf{(33)}$$

with $w_x = \frac{\pi_x}{\sum_y \pi_y}$, $0 \le w_x \le 1$. The definition for the solvent requirement *DR'* used here differs from the more widely applied definition (Eq. 22) to achieve homogeneous dimensions, thus ensuring dimensionless weights. Therefore *DR*' refers to the solvent mass consumed in one time unit (Δt = 1, day, $\rho_D = 1000 g/L$) instead of to the solvent flow rate, i.e.:

$$DR' = DR\, \rho_D\, \Delta t \quad \textbf{(34)}$$

On the other hand, in the following results will be given using the conventional definition for *DR* (Eq. 22) for the sake of clarity.

4.3.2. Role of enzyme requirement

In principle, two fundamentally different scenarios for the reactor operation can be envisioned depending on the cost contribution of the enzyme. When the enzyme cost is negligible, the reactor should be overloaded with enzyme in order to ensure practically complete conversion which in turn results in a racemic SMB feed – evidently the most favorable feed composition for SMB operation that can be achieved in an integrated setup. In consequence, the optimal operating point for the integrated process will not be different from the respective operating point for the stand-alone SMB. This corresponds to the modeling results presented above, where the stationary phase was implicitly assumed to be the major cost driver and the cost of enzyme was neglected.

If the costs for the biocatalyst cannot be neglected, the reactor should be operated with reduced conversion and hence the SMB feed concentration will be enriched with the distomer. On closer inspection this operation scenario leads to problematic consequences for the reaction-integrated process. First of all, the enzyme is subject to degradation and hence the pool of active enzyme is steadily decreasing which results in decreasing conversion in traditional isothermal operation. In consequence, the SMB is challenged with a dynamic change in feed concentration which might

require adaptation of SMB operating points during operation in order to ensure constant product purity. A recent work shows that product purities in a similar integrated process can be controlled by adjusting the retentate flow rate (Swernath et al., 2014): a similar approach can be envisioned for the integrated process concept presented in this work by reducing the feed flow rate.

In order to analyze the behavior of an integrated process where enzyme costs cannot be neglected, a two-objective Pareto set was generated with *PR* and *ER* as conflicting objectives (Fig. 9). The amount of enzyme (which for the previous simulations was kept constant) was added as a decision variable, specifically the enzyme concentration c_{ENZ}, while the reactor volume V_{EMR} was kept constant. The minimum level for c_{ENZ} was set to 2% of the maximal experimentally feasible concentration of 4.2 g L^{-1} (we did not include higher possible enzyme concentrations as this would require additional expensive enzyme work up).

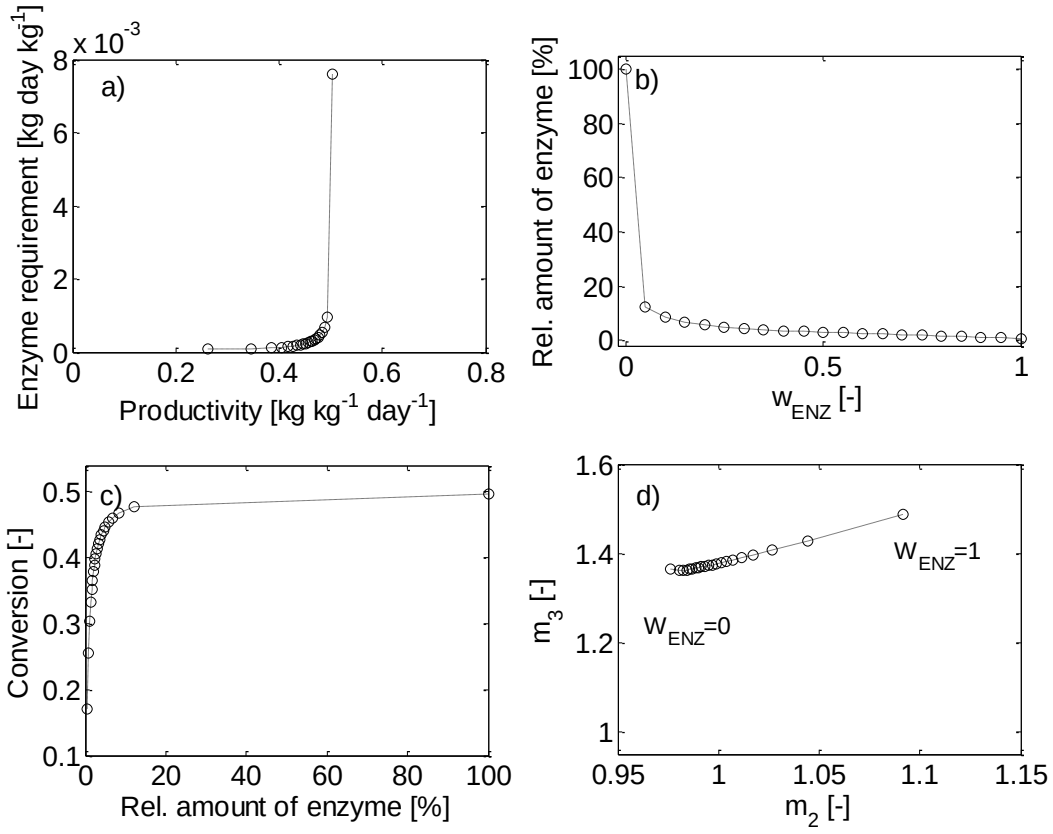

Fig. 9. Impact of enzyme concentration on process performance. a) Pareto curve with *PR* and *ER* as conflicting objectives. b) The corresponding relative enzyme amount and weight factor w_{ENZ}. c) Dependency of conversion on the relative amount of enzyme. d) Development of m-values with weight factor w_{ENZ}.

The substantial trade-off between the performance parameters *ER* and *PR* can be observed in Figs 9a and b. The distinct curvature of the Pareto set signifies that the enzyme concentration can be

drastically reduced with only a small compromise on productivity. This is due to the nature of the reversible Michaelis-Menten enzyme kinetics for which the driving force is the difference in concentration of the two enantiomers. With increasing conversion the concentration difference in the reactor decreases and consequently an increasing amount of enzyme is required to further increase the conversion. The actual enantiocomposition of the methionine leaving the EMR affects the SMB operating points. With increasing weight of the *ER*, conversion X is decreased. Consequently, the optimal m_2 and m_3 values increase (Fig. 9d) since the feasible region in the m_2-m_3 plane moves towards higher m_2-m_3 values with decreasing mass fraction of the stronger adsorbing component, as was first shown for Langmuir-type chromatographic systems (Mazzotti et al., 1997).

A similarly distinct Pareto curve results when *DR* and *ER* are used as objective functions (supplementary fig. S1). Thus summarizing, with decreasing enzyme requirement, the overall production rate is reduced, which results in a relative increase in *DR* since the absolute amount of solvent in order to regenerate the stationary phase is only marginally affected.

It is worth noting here that in an experimental implementation for an EMR with limited amount of catalyst, a suitable control device becomes necessary that uses the optimal conversion (depending on the specific operating point chosen from Fig. 9a) as a goal variable and the temperature (or fresh catalyst feed flow rate) as a control element becomes necessary.

4.3.3. Specific cost ranges and identification of cost-sensitive performance parameters

Process scale, purchase prices and stability of the applied materials are often not exactly known in the project development phase and may be subject to change. Consequently, reasonable price ranges should be compiled that then can be covered in the optimization procedure. For the specific case at hand, prices for the chiral stationary phase are assumed to vary between 75 000 $/kg, reflecting very small scale separation with small SMB columns, and 20 000 $/kg, representative of operation on larger scale. As the stability of the stationary phase is largely unclear a very cautious value of 50 days is assumed as lower limit and 2000 days as upper limit.

Table 2: Estimation of minimal and maximal weight factors for each unit operation.

	P_x [\$ kg^{-1}] or [\$ m^{-2}]		l_x [days]		π_x [\$ kg^{-1} day^{-1}] or [\$ m^{-2} day^{-1}]		w_x [-]	
	Min	**Max**	**Min**	**Max**	**Min**	**Max**	**Min**	**Max**
Enzyme	5000	50000	3	50	100	16667	0.06	1.00
Stationary Phase	20000	75000	50	2000	10	1500	0.00	0.94
Membrane	10	200	25	500	0.02	8	0.00	0.07
Solvent*	0.1	10	1	1	0.1	10	0.00	0.08

* The “life-span” of the solvent is defined by the time span applied in calculation of the solvent amount (Eq. 33)

The cost for the enzyme production depends on many factors including the scale of cultivation, the expression level in recombinant overproduction, intra-or extracellular production, and required degree of purification. Recently, a comprehensive cost analysis for the production of recombinant proteins was reported by Tufvesson et al. and suggested a price range of 5'000 to 50'000 \$ kg^{-1} for enzymes that can be expressed to high levels in the model bacterium *E. coli* (Tufvesson et al., 2010), which is the case for AAR (Bechtold et al., 2007b). The stability of wild-type AAR in aqueous/organic solvents is limited, so the enzyme can currently only be operated in the range of days (Bechtold et al., 2007b). Protein engineering methods can be applied to alleviate the stability limitation, often by an order of magnitude (Bechtold and Panke, 2012).

The prices for the membrane material were taken from online resources. Based on the estimated ranges for the prices and life-spans, the upper and lower limits for the weight factors were calculated (Table 2). Note that the cost contribution from the membrane was assumed to be negligible. In order to test this hypothesis we analyzed the distribution of costs for the scenario where the membrane costs were most pronounced ($w_{NFM,MAX}$=0.07, compare Table 2). The in-silico optimization results show that the NF cost contribution did not exceed 3% of the overall cost. Hence, in the following analysis the focus was put on cost for enzyme, stationary phase and solvent.

4.3.4. Cost analysis for *PR*, *DR* and *ER*

Based on the data collected in Table 2, a Pareto analysis was performed with the 3 objectives *PR, DR* and *ER*. All weight factors (w_{CSP}, w_{ENZ}, w_D) were varied from 0 to 1. Even though the upper limit of w_D was only 0.08 (Table 2), the full range was covered here, to give a broader overview. The resulting surface is shown in Fig. 10. It should be noted that the uneven distribution of the Pareto surface is a consequence of employing the traditional weighted sum method for multi-objective optimization. An adaptation of the weighted sum method (Kim and Weck, 2005) might lead to a more even distribution of the optimal points on the Pareto surface.

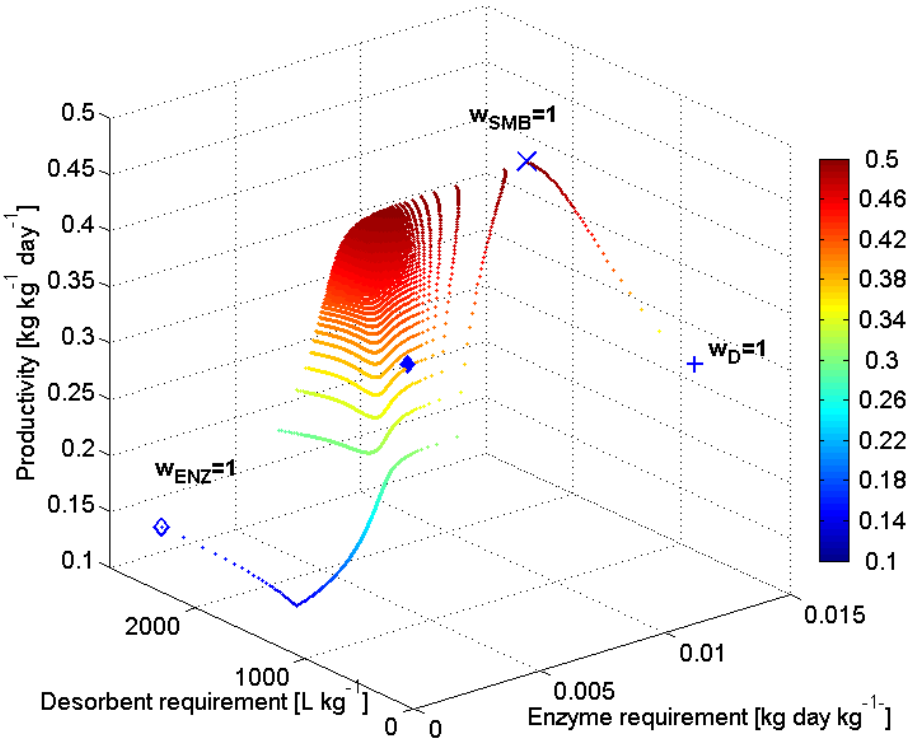

Fig.10. 3-dimensional Pareto set with *ER*, *DR* and *1/PR* as objective functions. The individual optimal operating points at the maximal respective w_x with absolute minimal enzyme requirement (diamond), minimal desorbent requirement (+) and maximal productivity (x) are indicated. The sample operating point corresponding to the weight values listed in Table 3 is indicated as filled diamond.

The individual optimal points for each of the 3 objectives at w_x=1 are all far removed from the swarm of optimal operating points. This further underlines the clear conflict between each of the objectives.

Based on the obtained performance values from the presented optimization and assuming for example a medium sized process (1 kg product per day) with prices and life-spans for the stationary phase (25,000 $/kg and 500 days), solvent (0.5 $/kg), enzyme (30,000 $/kg and 3 days) and membrane (100 $/kg and 100 days), the variable cost for 1 kg of D-Met is around 285 $ (Table 3).

Table 3: Estimation of absolute and relative cost contributions of the individual unit operations based on prices, life-spans and in-silico optimization results.

	P_x [\$ kg^{-1}] or [\$ m^{-2}]	l_x [days]	π_x [\$ kg^{-1} day^{-1}] or [\$ m^{-2} day^{-1}]	w_x [-]	Mx/TP [kg kg^{-1} day] or [m^2 kg^{-1} day] *	[\$ kg D-Met^{-1}]	[%]
Enzyme	30000	3	10000	0.99488	9.72E-04	10	3.4
Stationary Phase	25000	500	50	0.00497	2.585	129	45.4
Membrane	100	100	1	0.00010	0.050	0	0.0
Solvent	0.5	1	0.5	0.00005	291.180	146	51.2
*from Pareto optimization runs			10051.5		∑	285	

It is worth noting that in the case of the enzyme, the high weight is balanced by the low amount that is needed in the process. Conversely, the very low weight for the solvent is balanced by the high amount that is required. The corresponding operating point is shown in Fig. 10. The raffinate purity in this operating point is around 88%, and the conversion is 0.477. Remarkably, 40% of costs can be saved compared to an operating point with the same weights, but where recycling purity and conversion are fixed to the maximum value. Nevertheless, this cost is high, in particular as the examined starting materials L-Met or DL-Met are very cheap.

On the other hand, D-Met was selected as a model compound, and many advanced racemic starting materials in pharmaceutical synthesis are in the same order of magnitude as the calculated costs here, so the opportunity to obtain a yield close to 100% becomes attractive. Remarkably, the solvent shows the highest relative cost contribution of 51%, followed by stationary phase (45%). In the light of this result, it is worth noting that a solvent recycling should be envisioned as a next step in the development. Considering the apparently low cost of NF operation compared to the integrated process, another NF operation seems appropriate. The cost contribution for the enzyme in this model case is only 3.4%, which clearly demonstrates the feasibility of biocatalysis in chemical processes, even if the enzyme has not yet undergone directed evolution to improve its stability and thus its life-span is rather short.

5. Conclusion

In this work the experimental implementation of an integrated process for the production of single amino acid enantiomers from a racemate, employing continuous chromatography and biocatalysis, is presented for the first time. We demonstrate that this process can be operated in stable fashion for at least over 30 h despite i) highly non-linear adsorption isotherms, ii) the existence of a memory effect in the adsorption behavior of the CSP, and iii) the lack of sophisticated online control mechanisms that have been proposed for similar process combinations previously (Amanullah and

Mazzotti, 2006; Swernath et al., 2014). The experimental proof of concept run was designed employing the traditional complete separation criterion for the SMB, meaning that both outlet purities should be nearly absolute.

In terms of process stability, the life-span of the enzyme is clearly the limiting factor, and a large excess of biocatalyst was added to ensure constant conversion.

Next, an integrated process model was developed in order to analyze the effect of relaxed purity constraints on the performance indicators throughput and desorbent requirement, and yield. We showed that large savings of up to 60% solvent and 30% of stationary phase can be reached for a given throughput when the complete separation criterion is relaxed and the recycle purities are allowed to decrease.

A comprehensive Pareto analysis with productivity, desorbent requirement and enzyme requirement as objectives showed that large amounts of enzyme as well as solvent – which is the major cost driver in this model case – can be saved with little negative effect on productivity.

The design principles analyzed in this work (relaxed purity constraints and limited use of enzyme) can be generalized to a large number of process installations with SMB and Michaelis-Menten type reaction kinetics. We see potential for such integrated processes particularly for high-value products in the chemical and pharmaceutical industry, where the development time is the major limiting factor.

The estimated operating costs are relatively high which can be primarily attributed to the uncharacteristically low specific productivity and high solvent consumption of the SMB separation, which is easily a factor of 5 removed from productivities typically observed in industrial SMB process. Therefore, the presented numbers should not be considered as representative for this type of process, but should rather demonstrate that the proposed optimization strategy provides an estimate of the variable production cost which then can be used in a comprehensive investment cost analysis for evaluation of overall feasibility of the process. Finally major cost drivers are identified and the benefit of possible process improvements (e.g. by screening for a better enzyme or separation system) can be easily evaluated as by referring to the 3D pareto analysis which indicates areas of increased sensitivity towards cost weight distribution.

Acknowledgements

The authors wish to thank Prof. Malte Kaspereit and Subramanian Swernath for the introduction to the GAMS environment, and Prof. Marco Mazzotti for the provision of the equilibrium short cut model. This work was funded by the EU FP7 project INTENANT. Imthiyas NA Majeed assisted in conducting some of the experiments presented in this work.

Nomenclature

Symbol	Unit	Comment
A_{NF}	cm^2	Membrane area
b	$L\ g^{-1}$	Langmuir constant
c	$g\ L^{-1}$	Concentration in fluid phase
DR	$L\ kg^{-1}$	Desorbent requirement
ER	$kg\ day\ kg^{-1}$	Enzyme requirement
F	$kg\ day\ kg^{-1}$	objective function
k_{cat}	min^{-1}	Catalytic constant of racemization
K_M	$g\ L^{-1}$	Michaelis-Menten constant
m		Flow rate ratio
M	kg	Mass
MR	$m^2\ day\ kg^{-1}$	Membrane requirement
N		Number of stages
n_c		Number of SMB columns
P	$\$\ kg^{-1}$ or $\$\ m^{-2}$	Price
PC	$\$\ kg^{-1}$	Production cost
PR	$kg\ kg^{-1}\ day^{-1}$	Specific productivity
Pu	%	Purity SMB outlets
Q	$mL\ min^{-1}$	Volumetric flow rate
q	$g\ L^{-1}$	Concentration in solid phase
q_s	$g\ L^{-1}$	Saturation capacity
r	$g\ L^{-1}\ min^{-1}$	Reaction rate
REJ		Rejection
t^*	min^{-1}	Switch time
TP	$kg\ day^{-1}$	Throughput
V_C	mL	Column volume
VCF		Volume concentration factor
V_D	mL	Extra-column dead volume
w		Weight factor
X		Conversion in EMR
Y		Yield

Greek			
ε			Porosity
ρ		$g\ L^{-1}$	Density
Π	$\$\ kg^{-1}\ day^{-1}$		Specific cost per time
Δ			Feed node dilution factor

	Index	
C		Column
	CSP	Chiral stationary phase
	D0	Desorbent
	E	SMB extract
	EMR	Enzyme membrane reactor
	ENZ	Enzyme
	F	SMB feed
	F0	Process feed
	i	Components, 1=L-Met, 2=D-Met
	j	SMB section
	k	Stage index
	NFM	Nanofiltration membrane
	PER	Nanofiltration permeate
	R	SMB raffinate
	RET	NF retentate
	X	Unit index

References

Ager, D. J., de Vries, A. H. M., de Vries, J. G., 2012. Asymmetric homogeneous hydrogenations at scale. Chemical Society Review 41, 3340–3380

Amanullah, M., Mazzotti, M., 2006. Optimization of a hybrid chromatography-crystallization process for the separation of Tröger's base enantiomers. Journal of Chromatography A 1107, 36-45.

Bechtold, M., Felinger, A., Held, M., Panke, S., 2007a. Adsorption behavior of a teicoplanin aglycone bonded stationary phase under harsh overload conditions. Journal of Chromatography A 1154, 277-286.

Bechtold, M., Heinemann, M., Panke, S., 2006. Suitability of teicoplanin–aglycone bonded stationary phase for simulated moving bed enantioseparation of racemic amino acids employing composition-constrained eluents. Journal of Chromatography A 1113, 167-176.

Bechtold, M., Makart, S., Reiss, R., Alder, P., Panke, S., 2007b. Model-based characterization of an amino acid racemase from Pseudomonas putida DSM 3263 for application in medium-constrained continuous processes. Biotechnology and Bioengineering 98, 812-824.

Bechtold, M., Panke, S., 2012. 7.5 Reaction Engineering of Biotransformations, in: Editors-in-Chief: Erick, M.C., Hisashi, Y. (Eds.), Comprehensive Chirality. Elsevier, Amsterdam, pp. 71-100.

Bhaskar, V., Gupta Santosh, K., Ray Ajay, K., 2000. Applications of multiobjective optimization in chemical engineering, Reviews in Chemical Engineering 16, 1-54

Biressi, G., Ludemann-Hombourger, O., Mazzotti, M., Nicoud, R.-M., Morbidelli, M., 2000. Design and optimisation of a simulated moving bed unit: role of deviations from equilibrium theory. Journal of Chromatography A 876, 3-15.

Blaser, H.-U., 2002. The chiral switch of (S)-metolachlor: A personal account of an industrial odyssey in asymmetric catalysis. Advanced Synthesis & Catalysis 344, 17-31.

Blehaut, J., Nicoud, R.-M., 1998. Recent aspects in simulated moving bed. Analusis 26, 60-70.

Chankvetadze, B., 2012. Recent developments on polysaccharide-based chiral stationary phases for liquid-phase separation of enantiomers. Journal of Chromatography A 1296, 26-51.

Federsel, H.-J., 2009. Chemical process research and development in the 21st century: challenges, strategies, and solutions from a pharmaceutical industry perspective. Accounts of Chemical Research 42:671-680.

Francotte, E.R., 2001. Enantioselective chromatography as a powerful alternative for the preparation of drug enantiomers. Journal of Chromatography A 906, 379-397.

Fuereder, M., Majeed, I.N., Panke, S., Bechtold, M., 2014. Model-based identification of optimal operating conditions for amino acid simulated moving bed enantioseparation using a macrocyclic glycopeptide stationary phase. Journal of Chromatography A 1346, 34-42.

Fuereder, M., Panke, S., Bechtold, M., 2012. Simulated moving bed enantioseparation of amino acids employing memory effect-constrained chromatography columns. Journal of Chromatography A 1236, 123-131.

Gedicke, K., Kaspereit, M., Beckmann, W., Budde, U., Lorenz, H., Seidel-Morgenstern, A., 2007. Conceptual design and feasibility study of combining continuous chromatography and crystallization for stereoisomer Separations. Chemical Engineering Research and Design 85, 928-936.

Gentilini, A., Migliorini, C., Mazzotti, M., Morbidelli, M., 1998. Optimal operation of simulated moving-bed units for non-linear chromatographic separations: II. Bi-Langmuir isotherm. Journal of Chromatography A 805, 37-44.

Hashimoto, K., Adachi, S., Noujima, H., Ueda, Y., 1983. A new process combining adsorption and enzyme reaction for producing higher-fructose syrup. Biotechnology and Bioengineering 25, 2371-2393.

Kaspereit, M., Jandera, P., Škavrada, M., Seidel-Morgenstern, A., 2002. Impact of adsorption isotherm parameters on the performance of enantioseparation using simulated moving bed chromatography. Journal of Chromatography A 944, 249-262.

Kaspereit, M., Seidel-Morgenstern, A., Kienle, A., 2007. Design of simulated moving bed processes under reduced purity requirements. Journal of Chromatography A 1162, 2-13.

Kaspereit, M., Swernath, S., Kienle, A., 2012. Evaluation of competing process concepts for the production of pure enantiomers. Organic Process Research & Development 16, 353-363.

Kim, I.Y., Weck, O.L., 2005. Adaptive weighted sum method for multiobjective optimization: a new method for Pareto front generation. Structural and Multidisciplinary Optimization 31, 105-116.

Leuchtenberger, W., Huthmacher, K., Drauz, K., 2005. Biotechnological production of amino acids and derivatives: current status and prospects. Applied Microbiology and Biotechnology 69, 1-8.

Martin, A.J., Synge, R.L., 1941. A new form of chromatogram employing two liquid phases: A theory of chromatography. 2. Application to the micro-determination of the higher monoamino-acids in proteins. Biochemical Journal 35, 1358-1368.

Martin, G., Pereira, C., Pettersson, F., Saxen, H., Murzin, D. Y., Rodrigues, A., Salmi, T., 2015. Combining reaction and separation in heterogeneous catalytic hydrogenation of ethylformate. Chemical Engineering and Technology 38, 804-812.

Mazzotti, M., Storti, G., Morbidelli, M., 1997. Optimal operation of simulated moving bed units for nonlinear chromatographic separations. Journal of Chromatography A 769, 3-24.

Mazzotti, M., 2006. Design of simulated moving bed separations: Generalized Langmuir isotherm. Industrial Engineering & Chemistry Research 45, 6311-6324.

Nimmig, S., Kaspereit, M., 2013. Continuous production of single enantiomers at high yields by coupling single column chromatography, racemization, and nanofiltration. Chemical Engineering and Processing: Process Intensification 67, 89-98.

Palacios, J.G., Kramer, B., Kienle, A., Kaspereit, M., 2011. Experimental validation of a new integrated simulated moving bed process for the production of single enantiomers. Journal of Chromatography A 1218, 2232-2239.

Paredes, G., Mazzotti, M., 2007. Optimization of simulated moving bed and column chromatography for a plasmid DNA purification step and for a chiral separation. Journal of Chromatography A 1142, 56-68.

Rajendran, A., Paredes, G., Mazzotti, M., 2009. Simulated moving bed chromatography for the separation of enantiomers. Journal of Chromatography A 1216, 709-738.

Sambrook, J., Russell, D.W., 2001. Molecular Cloning : A Laboratory Manual, 3rd ed ed. Cold Spring Harbor Laboratory Press, Cold Spring Harbor, N.Y.

Sheldon, R.A., 1996. Chirotechnology: Designing economic chiral syntheses. Journal of Chemical Technology & Biotechnology 67, 1-14.

Swernath, S., Kaspereit, M., Kienle, A., 2014. Coupled continuous chromatography and racemization processes for the production of pure enantiomers. Chemical Engineering & Technology 37, 643-651.

Trost, B.M., 2004. Asymmetric catalysis: An enabling science. Proceedings of the National Academy of Sciences of the United States of America 101, 5348-5355.
Tufvesson, P., Lima-Ramos, J., Nordblad, M., Woodley, J.M., 2010. Guidelines and cost analysis for catalyst production in biocatalytic processes. Organic Process Research & Development 15, 266-274.

Siitonen, J., Mänttäri, M., Seidel-Morgenstern, A., Sainio, T., 2015. Robustness of steady state recycling chromatography with an integrated solvent removal unit. Journal of Chromatography A 1391, 31-39.

von Langermann, J., Kaspereit, M., Shakeri, M., Lorenz, H., Hedberg, M., Jones, M.J., Larson, K., Herschend, B., Arnell, R., Temmel, E., Bäckvall, J.-E., Kienle, A., Seidel-Morgenstern, A., 2012. Design of an integrated process of chromatography, crystallization and racemization for the resolution of 2',6'-pipecoloxylidide (PPX). Organic Process Research & Development 16, 343-352.

Wagner, N., Fuereder, M., Bosshart, A., Panke, S., Bechtold, M., 2012. Practical aspects of integrated operation of biotransformation and SMB separation for fine chemical synthesis. Organic Process Research & Development 16, 323-330.

Ward, R.S., 1995. Dynamic kinetic resolution. Tetrahedron: Asymmetry 6, 1475-1490.

Würges, K., Petruševska-Seebach, K., Elsner, M.P., Lütz, S., 2009. Enzyme-assisted physicochemical enantioseparation processes—Part III: Overcoming yield limitations by dynamic kinetic resolution of asparagine via preferential crystallization and enzymatic racemization. Biotechnology and Bioengineering 104, 1235-1239.

Zhu, A., Long, F., Wang, X., Zhu, W., Ma, J., 2007. The negative rejection of H^+ in NF of carbonate solution and its influences on membrane performance. Chemosphere 67, 1558-1565.

Supplementary figure

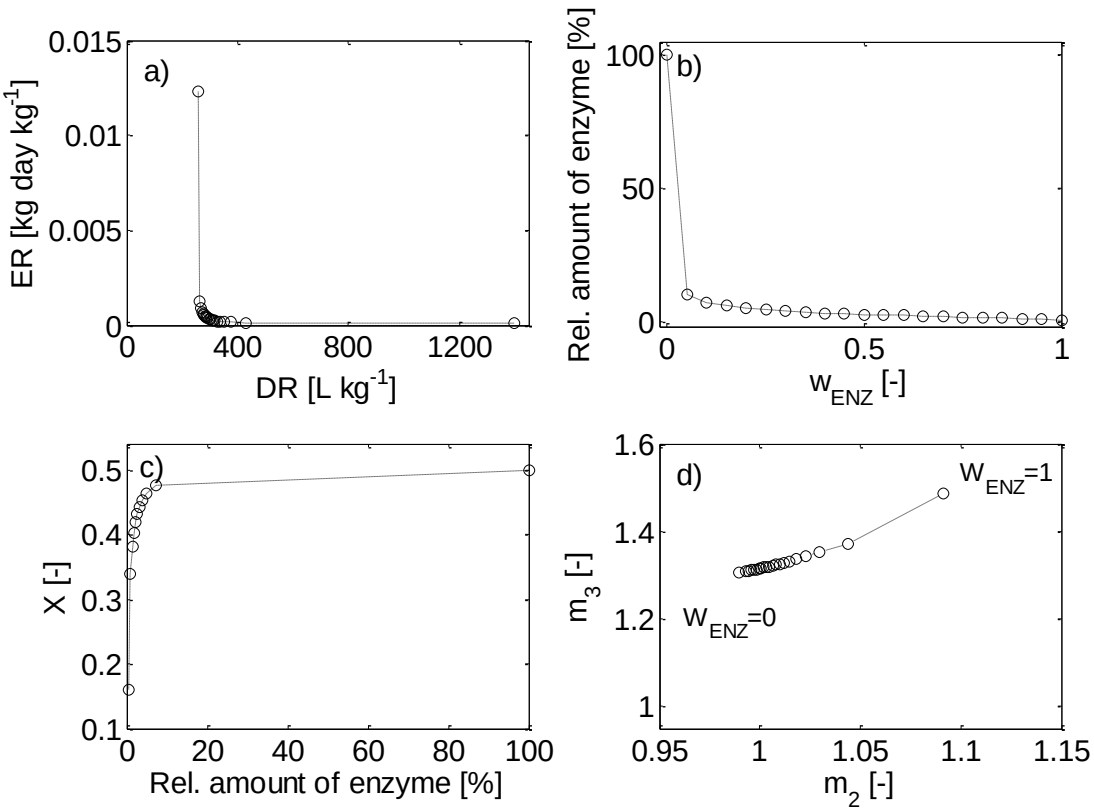

Fig. S1. Influence of enzyme amount on process performance parameters *ER* and *DR*. a) Pareto curve with *DR* and *ER* as conflicting objectives. b) Development of relative amount of enzyme with increasing weight factor w_{ENZ}. c) Dependency of conversion *X* on the relative amount of enzyme. d) SMB *m*-values dependency on weight factor w_{ENZ}.